ANALYTICAL MODEL SENSITIVITY STUDY FOR AEROELASTIC STABILITY OF STRAIGHT AND SWEPT-TIP ROTOR BLADES

Thomas H. Maier

Army/NASA Rotorcraft Division
Aeroflightdynamics Directorate (AMRDEC)
US Army Aviation and Missile Command
Ames Research Center,
Moffett Field, California

Anita I. Abrego

Army/NASA Rotorcraft Division
National Aeronautics & Space
Administration
Ames Research Center,
Moffett Field, California

Abstract

A sensitivity study was undertaken to improve the correlation between experiment and analysis for the regressing lag mode damping of two small-scale aeroelastic stability experiments. The experiments were conducted using isolated, hingeless rotors with identical fiber-reinforced composite root flexures, operated in hover and forward flight at tip speeds approximating those of full-scale helicopters. The rotors differed in blade planform and structure. The first blade set had rectangular planform with soft blade structure. The second set had blades of stiffer construction with swept tips. The sensitivity study examined parameters in the experimental test set-up and the analytical model for the source of poor correlation. A single airspeed sweep for each experiment was analyzed to assess the sensitivity to each parameter. An improved analytical model was created using the same modeling improvements for both rotors and an extensive range of test conditions was calculated with the new models. Significant improvement was seen in the correlation for the swept-tip rotor while no corresponding improvement was seen for the straight blade rotor.

1   Introduction

Validation of helicopter comprehensive codes is an important step in establishing their usefulness to the design community. These efforts are usually taken in many steps testing structural, structural dynamic and aerodynamic theories. Beam models may be compared with measurements such as those made in the Princeton beam experiment[1] and dynamic stall models may be compared with measurements such as those made in Piziali's oscillating wing experiment.[2] These simple, well-controlled experiments provide a strong basis for applying a given analysis to a new problem.

The U.S. Army Aeroflightdynamics Directorate (AFDD) has conducted a series of aeroelastic and aeromechanical small-scale rotor stability tests designed to provide data suitable for validation of analyses. This body of work was recently extended to include hover and forward flight testing of an isolated, hingeless rotor with swept-tip blades at realistic tip speeds.[3] This test built directly on the work completed in 1995 for a hingeless rotor with straight blades.[4] Both rotors share the same hub and root flexure design; however, the blade structure was significantly altered to produce swept-tip blades which could be tested over the same range of collective pitch angles and advance ratios as the rotor with straight blades.

Reference 3 presented test data for the swept-tip rotor, showed comparisons with the straight blade rotor data and showed the level of correlation between both data sets and calculations using the comprehensive rotorcraft code CAMRAD II.[5] The correlation in forward flight was generally good; however, it degraded significantly at moderate and high advance ratios for the swept-tip rotor at the higher thrust levels, and at moderate advance ratios with low thrust for the straight blade rotor.

This paper presents an analytical sensitivity study of structural, inertial and aerodynamic modeling parameters undertaken to identify the cause of the degraded correlation seen in reference 3. An airspeed sweep was chosen for each rotor to investigate the sensitivities over a range of airspeeds. The shaft angle, collective pitch angle and precone angle were chosen to provide conditions where the correlation between data and analysis was poor. This resulted in operating conditions that were not consistent between the two rotors but provided a difficult test for the analysis. The sensitivity study investigated details of the experimental test hardware and of the analytical structural dynamic and aerodynamic models.

2   Rotor Experiments

The rotor systems for the straight blade and swept-tip rotors were 7.5-foot diameter small-scale hingeless rotors with 3.4-inch NACA 0012 airfoil sections and zero twist. A planform view of the blades was shown in figure 1. The nominal rotor speed of 1700 RPM resulted in a Reynolds number of 1.2 x 10^6, and a Mach number of 0.60 at the blade tip in hover. The blades had no dampers and were tested with a 0° and a 2° precone hub. The non-dimensional flap, lag and torsion frequencies were 1.13, 0.71 and 2.62 for the straight blades and 1.12, 0.66 and 2.85 for the swept-tip blades. All blades were instrumented with flap, lag and torsion bridges at 12% span on the root flexure. The swept-tip blade had 30° of sweep which started at 90% span with the 3.4 inch NACA 0012 airfoil section translated back to the swept position.

The test conditions were defined by shaft angle, collective pitch angle, advance ratio and hub precone angle. Rotor cyclic pitch was adjusted to minimize the 1/rev flap bending moment at the 12% span location. Once operating at a steady test condition the rotor was excited at the regressive lag frequency by a single non-rotating cyclic control actuator. Time history data were acquired during the decay. Damping of each individual blade and of the cyclic multi-blade coordinate[6] were calculated using a Moving-Block analysis.[7,8] Figure 2 shows the rotor with the swept-tip blades on the small-scale Rotor Test Rig (RTR) in the Army/NASA 7- by 10-Foot Wind Tunnel at Ames Research Center. A more detailed description of the tests may be found in references 3 and 4.

3   Baseline Analytical Models

The CAMRAD II analysis was used to calculate the trim solution and the linearized eigenanalysis about the trim equilibrium solution. The periodic equations were solved using Floquet-Lyaponov Theory. Multiblade coordinates were used to calculate rotor modes in the fixed system.

The structural model for both rotors had the same number of elastic elements. The blades had two elements in the flexure section and four elements distributed along the remainder of the blade, where the last element was 10% of span resulting in a single element for the swept region. Each of the structural elements contained 3 axial, 2 lag, 2 flap and 2 torsion elastic degrees of freedom. Twelve rotating blade modes were calculated using finite element analysis and used for the trim equilibrium solution and the eigenanalysis. Modal structural damping was adjusted individually for each rotor to agree with the hover measurements near 0° collective pitch angle. The values of modal damping in units of percent critical damping were 0.38 for the straight blade and 0.32 for the swept-tip blade.

The aerodynamic model divided the airfoil section into 15 aerodynamic segments and a NACA 0012 C81 airfoil table provided lift, drag and moment as a function of angle of attack and Mach number. The baseline calculation for hover used uniform inflow with a hover inflow correction factor equal to 1.1, tip loss equal to 0.98 and a momentum theory dynamic inflow model.[5] Forward flight calculations were made with a free wake and the Pitt and Peters dynamic inflow actuator disk theory.[5]

Trim was achieved with fixed advance ratio, shaft angle and collective pitch angle. The cyclic pitch inputs were adjusted using a Newton-Raphson iteration until zero pitch and roll moments were achieved.

4   Baseline Forward Flight Correlation

Shortly after the swept-tip rotor test was completed a correlation study was undertaken and reported in reference 3. The baseline CAMRAD II model described in the preceding paragraphs was used for that study. Calculations were made for an extensive

range of operating conditions shown here in tables 1 and 2. The resulting correlation is shown for the straight blade and swept-tip rotors in figures 3 and 4, respectively. In the figures the calculated regressing lag mode damping coefficient (or damping exponent) was plotted versus the measured damping coefficient. Perfect correlation falls on the 45° line passing through the origin. A 20% error wedge has been added to these figures as an indication of what the authors believe to be an acceptable error for rotor design purposes. Both figures show regions where the correlation was outside the desired error wedges. Correlation coefficients provide a quantitative measure of the correlation. The resulting correlation coefficients were 0.91 for the straight blade rotor and 0.71 for the swept-tip blade rotor. The intent of the sensitivity study was to determine a physical explanation for the poor correlation, or to find improvements to the analytical model that will bring the correlation inside the error wedge.

Since the correlation seen in figures 3 and 4 varied with the rotor operating condition, it was desirable to conduct the sensitivity study over a range of operating conditions. Figures 5 and 6 show a comparison of calculated and measured damping for several advance ratio sweeps. These figures contain a subset of the data in figures 3 and 4 and, therefore, have different correlation coefficients. The correlation coefficients for the data in these advance ratio sweeps were 0.91 and 0.31 for the straight blade and swept-tip rotors, respectively. Figures 5 and 6 contain the operating conditions with the worst correlation, with the exception of two collective pitch angle sweeps at fixed advance ratio in figure 4 (curves with dot in the center of their symbols). The discrepancies between measurement and analysis in figure 6 showed a monotonic increase in the error with collective pitch angle. However, the errors with advance ratio suggested that something was missing from the physics of the model. The measurements showed an increase in damping from $\mu = 0.1$ to $\mu = 0.2$, then the slope decreased and the damping decreased to a minimum near $\mu = 0.35$, after which the damping increased again. This trend was not seen in the calculations which increased rapidly from $\mu = 0.1$ to $\mu = 0.3$ and continued to increase at a slightly lower rate. Because this trend was not captured by the analysis, airspeed sweeps were chosen for the sensitivity study. It is seen in figures 3 and 5, for the straight blade rotor,

Table 1. Straight blade rotor operating conditions in terms of an advance ratio range at specified precone angle, collective pitch angle and shaft angle for which calculations were made.

$\beta_p = 2°$	$\alpha_s = -6°$	$\alpha_s = -3°$	$\alpha_s = 0°$
$\theta_o = 2.9°$	.00 - .31	.01 - .31	.00 - .31
$\theta_o = 3.8°$	.00 - .31	-	-
$\theta_o = 4.8°$	.00 - .33	-	-
$\theta_o = 5.9°$	.04 - .36	-	-

Table 2. Swept-tip rotor operating conditions in terms of an advance ratio range at specified precone angle, collective pitch angle and shaft angle for which calculations were made.

$\beta_p = 0°$	$\alpha_s = -6°$	$\alpha_s = -3°$	$\alpha_s = 0°$
$\theta_o = 2°$	-	-	.30
$\theta_o = 3°$	-	-	.00 - .46
$\theta_o = 4°$	-	-	.00 - .46
$\theta_o = 5°$	-	-	.01 - .46
$\theta_o = 6°$	-	-	.10 - .46
$\theta_o = 7°$	-	-	.15 - .41
$\theta_o = 8°$	-	-	.30
$\beta_p = 2°$ $\theta_o = 3°$	.02 - .46	.00 - .47	.01 - .46

that the worst correlation occurred at the highest collective pitch angle and the highest advance ratio. Therefore, the straight blade rotor 6° collective pitch angle speed sweep (shown as a heavy line in figures 3 and 5) was chosen for the sensitivity study. In figures 4 and 6, for the swept-tip rotor, it is again seen that the worst correlation occurs at the highest collective pitch angle. However, here the moderately high advance ratio ($\mu = 0.35$) was where the error was greatest. Although the correlation for the 7° collective pitch angle was the worst, the 6° collective pitch angle sweep (shown as a heavy line in figures 4 and 6) was chosen because the test data had a greater range of advance ratio.

These two airspeed sweeps were used throughout the sensitivity study to assess different parameters and modeling features. These sweeps are not an indication of the damping differences between straight and swept-tip rotor blades because the operating conditions

are not comparable. Although both sweeps were at 6° collective pitch angle, the shaft angles and precone angles were both different. The straight blade rotor had the 2° precone hub and the shaft was inclined forward 6° causing the rotor thrust to reduce with advance ratio, while the swept-tip rotor had the 0° precone hub and the shaft was not inclined.

5 Hover Sensitivity

Prior to looking at the sensitivity of the regressive lag mode damping to different parameters in forward flight a single parametric variation in hover provided insight into the differences between these two rotors. The measurements in hover showed much lower damping as a function of collective pitch angle for the swept-tip rotor than for the straight blade rotor. It was seen, in reference 3 that the CAMRAD II hover calculations for both rotors agreed well with the experiments. It was expected that the source of the damping difference could be determined with the help of the analysis.

Both straight and swept-tip rotor blades were designed to have the total center of gravity of the blade near the quarter chord. This was accomplished by placing small weight segments near the airfoil leading edge along the entire blade length for the straight blade rotor and along the unswept portion of the swept-tip blade. To balance the aft weighting of the swept portion of the blade a large balance weight was placed in the nose area of the airfoil near the 90% span station as shown in figure 7. This balance weight was approximately 13% of the total blade weight. The mass of this balance weight was found to be responsible for the damping difference between the two blade sets.

Figure 8 shows the parametric variation of this balance weight. In the figure the regressing lag mode damping coefficient was shown as a function of collective pitch angle. The symbols show the test data and the lines show the CAMRAD II calculations. Agreement between the experiment and the baseline calculations was very good. The baseline swept-tip rotor model was then adjusted incrementally. With the balance weight mass set to 3/4 of the original value, the damping level moved up toward the straight blade damping level. Calculations with 1/2 of the balance weight mass further increased the damping level. When calculations were made with 1/4 of the balance

weight mass the analysis would not converge, possibly due to flutter instability. Calculations were made with the planform of the swept-tip rotor and the structural and mass properties (i.e. no large balance weight) of the straight blade. These calculations produced damping slightly below, but very near the straight blade results. Finally, calculations were made with the planform and structure of the straight blade rotor with the addition of the swept-tip balance weight. These calculations produced damping nearly equal to the swept-tip rotor results, indicating that the inertial properties, which were dominated by the large balance weight rather than the tip sweep, were responsible for the significant difference in the damping of these two rotors.

6 Forward Flight Sensitivity

The forward flight sensitivity study was aimed specifically at improving the correlation over the entire range of conditions for both rotors. Although a single airspeed sweep for each rotor was used to assess the sensitivity to each parameter, the full range of operating conditions shown in tables 1 and 2 were used to determine the overall improvement.

The parametric changes to the analytical models have been categorized as experimental or analytical model parameters. The experimental model parameters were aimed at assessing model set-up errors and experimental measurement errors as well as blade-to-blade differences. The analytical model parameters were aimed at assessing different aerodynamic or structural dynamic models. The findings from the analytical model parameters should be universal to both rotors and extend potentially to the general design problem, while the experimental model parameters were specific to each test.

6.1 Experimental Model Parameter Results

As with all rotor tests that have more than one blade, there are small differences from blade to blade. These differences were measured to the extent possible for the straight blade rotor. Stiffness, total mass, total center of gravity, total polar moment of inertia, blade section mass, blade section center of gravity and blade section polar moment of inertia were all measured for each blade. The magnitudes of the parametric changes were chosen to encompass the differences measured

between the blades. The analytical parameters varied were: chordwise center of gravity location, chordwise tensile axis location, bending and torsion stiffness, blade mass, blade polar moment of inertia, root sweep angle, root droop angle, torque offset and aerodynamic center location.

The results for these variations are shown for the straight and swept-tip rotors in figures 9 through 13. It is seen in the figures that the straight blade rotor was more sensitive than the swept-tip rotor to the parameters studied. Both rotors were sensitive to the chordwise center of gravity location (figure 9), torque offset (figure 12) and the aerodynamic center location (figure 13).

There was no single parameter that appeared to improve the calculation substantially. Moving the center of gravity aft, adding a torque offset and moving the aerodynamic center forward for the straight blade rotor all appear to have the capability to improve the shape of the curve with advance ratio. However, they all increased the damping level above the measurements. It appears that these parameters (with a tuned magnitude), in combination with something which moves the whole curve down such as reducing the structural damping, would improve the correlation.

None of the parameters studied appeared to improve the shape of the damping curve for the swept-tip rotor. All the parameters essentially caused a shift up or down from the baseline curves.

6.2 Analytical Model Parameter Results

The analytical model parameter study offered a wide range of possible variations. It also offered the potential to point toward improvements that could be universal to all rotors. In some cases, however, a change was made just to see the influence of a given parameter, not as a viable improvement to the model. The parameters varied included: the number of structural elements, the effect of dynamic inflow, the effect of the wake model in capturing the trim deflections, the effect of the wake model in capturing the inflow velocity, incompressible aerodynamics and no stall. In contrast to the experimental model parameters, the swept-tip rotor was more sensitive

than the straight blade rotor to some of the analytical model parameters.

Figure 14 shows the importance of the number and location of the structural elements. The baseline models contained two elements in the flexure section, an element in the inboard transition, and three elements for the remainder of the blade. The most outboard element extended from 0.90 r/R to the tip so that the swept portion was a single element. One by one, elements were added to the flexure section until there was a total of five elements. A significant change was seen in the damping with the addition of the first element. Successive additions did not cause a significant change. An element was added to the blade with four elements in the flexure section and no significant change was seen. It was seen that the swept-tip blade was more sensitive to the number of elements modeling the flexure than was the straight blade.

Figure 15 shows the influence of the dynamic inflow model. The inclusion of dynamic inflow had a slight effect on the damping. As with the number of elements, the swept-tip rotor was more sensitive to the inclusion of dynamic inflow than was the straight blade rotor.

Figures 16 and 17 examine the importance of the wake model on two different aspects of the eigenanalysis. Both figures show comparisons with three wake models: uniform inflow, prescribed wake and free wake. In figure 16 the eigenanalysis was solved using the trim deflections from the three trim wake models, however, in all cases, the inflow velocity distribution came from the uniform inflow model. In figure 17 the eigenanalysis was solved with the deflections and the inflow velocity distribution from the trim wake models.

Figure 16 shows a significant change in the damping of the straight blade rotor when the deflected shape came from the prescribed or free wake model rather than the uniform inflow model. The swept-tip rotor did not show a similar sensitivity.

Figure 17 shows no significant change from figure 16 for the straight blade rotor, indicating that the changes in the induced velocity due to these different wake models did not effect the damping of this rotor in these

flight conditions. There was a significant change in the damping of the swept-tip rotor when the inflow velocity from the prescribed or free wake model was used rather than the uniform inflow model. Taken together, figures 15, 16 and 17 suggest that the best analytical model uses a vortex lattice model such as the prescribed or free wake models for the trim deflections and for the induced velocity distribution used in the eigenanalysis.

Figure 18 shows the influence of compressibility and stall on the calculation by removing their effects from the models. The incompressible calculation substituted zero for the calculated Mach number when entering the airfoil tables for lift, drag and moment coefficient. The "no stall" model suppressed stall by using a linear lift curve slope. The damping was reduced with incompressible aerodynamics. This was probably due to the reduced thrust from the lower lift coefficients obtained when entering the airfoil tables with zero Mach number. It was seen that modeling compressibility improved the level of the damping curve and the shape of the curve with advance ratio for both rotors. No difference was seen between the baseline calculations and the "no stall" calculations. Above 0.35 advance ratio the no stall calculation did not converge. This was probably caused by the high angles of attack in the reverse flow region.

7   Improved Forward Flight Correlation

The findings of the sensitivity study were used to establish an improved analytical model. Although the experimental model parameter investigation indicated input changes that may improve the correlation, there was no scientific justification, such as new mass properties measurements, to make such changes. There were, however, analytical model parameters that clearly showed shortcomings of the baseline models. Two structural elements in the flexure section were seen to be inadequate, since the result had not converged to the results obtained with more elements. It appeared that at least three elements in the flexure section were required. In the aerodynamic model it appeared that the prescribed or free wake model must be used to generate the deflected shape and the inflow velocity distribution for the eigenanalysis. To accomplish this dynamic inflow was turned off. The results of the sensitivity study indicate that this was an acceptable compromise, since dynamic inflow did not significantly effect the calculation.

The improved models were created and calculations were made for the same range of operating conditions as calculated for the baseline models (tables 1 and 2). Figures 19 and 20 show the correlation with the improved models for the straight blade and swept-tip rotors, respectively. The correlation for the straight blade rotor appeared to have degraded somewhat, although the differences between figure 19 and the baseline model in figure 3 were small. Significant improvement was seen in the correlation for the swept-tip rotor. The correlation coefficients with the improved models were 0.87 for the straight blade rotor and 0.93 for the swept-tip blade rotor. The result for the swept-tip rotor in figure 20 showed a significant improvement in the correlation coefficient and the curves were nearly within the desired error wedge.

The hover calculations were run with the additional structural element in the flexure section. The results were nearly identical to the original baseline calculation. Reference 4 showed the importance of dynamic inflow for the hover calculation, so it was retained in the calculation.

The two families of advance ratio sweeps at different collective pitch angles are shown in figures 21 and 22. As with figures 5 and 6, these figures contain a subset of the data in the correlation plots and, therefore, had different correlation coefficients. The correlation coefficients for the data in these advance ratio sweeps were 0.92 and 0.88 for the straight blade and swept-tip rotors, respectively. The new model for the straight blade rotor showed improvement over the baseline calculation of figure 5 at the highest advance ratio points and over the entire advance ratio range at 6° collective pitch angle. Agreement with the test data was worse for the other collective pitch angles over all but the highest advance ratio points. The improvement seen for the swept-tip rotor was much more significant. The damping at all collective pitch angles over the entire advance ratio range agreed better with the measured data. The up-down-up character of the measurements with advance ratio for the swept-tip rotor, however, was still not seen with the improved model.

8 Conclusions

The CAMRAD II analysis was used to assess the sensitivity of the regressing lag mode damping for two research rotors to various changes in the test hardware and the analytical modeling.

1. The substantial difference in damping between the two rotors in hover results from inertial differences in the rotors, primarily resulting from the balance weight near 90% span on the swept-tip blade.
2. The straight blade rotor showed significantly greater sensitivity than the swept-tip rotor to the experimental model parameters examined in this study.
3. The refined analytical model with more structural elements and the inflow velocity from a vortex lattice model significantly improved the correlation for the swept-tip rotor.
4. The up-down-up variation in the measured damping curve with advance ratio for the swept-tip rotor was not captured by the analysis.

9 References

1. Dowell, E.H.; Traybar, J. and Hodges, D.H., "An Experimental-Theoretical Correlation Study of Non-linear Bending and Torsion Deformations of a Cantilever Beam," *Journal of Sound and Vibration*, Vol. 50, No. 4, 1977.
2. Piziali, R.A., "2-D and 3-D Oscillating Wing Aerodynamics for a Range of Angles of Attack Including Stall," NASA TM 4632, September 1994.
3. Maier, Thomas H.; Sharpe, David L. and Abrego, Anita I., " Aeroelastic Stability for Straight and Swept-Tip Rotor Blades in Hover and Forward Flight," American Helicopter Society 55th Annual Forum Proceedings, Montreal, Canada, May 1999.
4. Maier, Thomas H.,; Sharpe, David L., and Lim, Joon W., "Fundamental Investigation of Hingeless Rotor Aeroelastic Stability, Test Data and Correlation," American Helicopter Society 51st Annual Forum Proceedings, Fort Worth, TX, May 1995.
5. Johnson, W., "Technology Drivers in the Development of CAMRAD II," American Helicopter Society, Aeromechanics Specialists Meeting, San Francisco, California, January 1994.
6. Hohenemser, Kurt H. and Yin, Sheng-Kuang, "Some Applications of the Method of Multiblade Coordinates," *Journal of the American Helicopter Society*, Vol. 17, No. 3, July 1972.
7. Hammond, Charles E. and Doggett, Robert V., Jr., "Determination of Subcritical Damping by Moving-Block/Randomdec Application," NASA Symposium on Flutter Testing Techniques, NASA SP-415, October 1975.
8. Bousman W.G. and Winkler D.J., "Application of the Moving-Block Analysis," Proceedings, AIAA/ASME/ASCE/AHS 22nd Structures, Structural Dynamics, and Materials Conference, Atlanta, Georgia, April 1981.
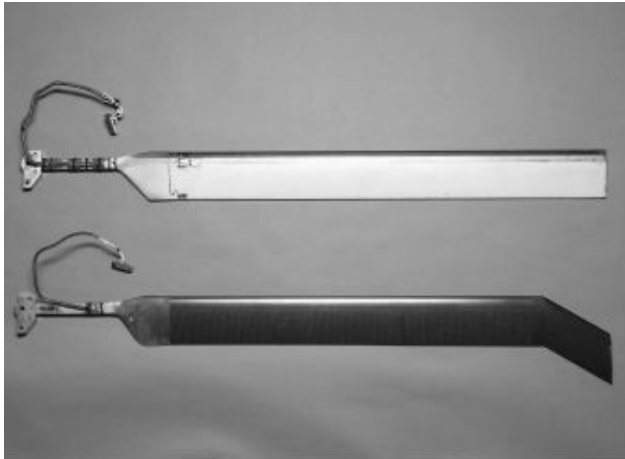
Fig. 1   Straight and swept-tip instrumented rotor blades.

Fig. 2   Swept-tip rotor on RTR test stand in the Army/NASA 7- by 10-Foot Wind Tunnel.
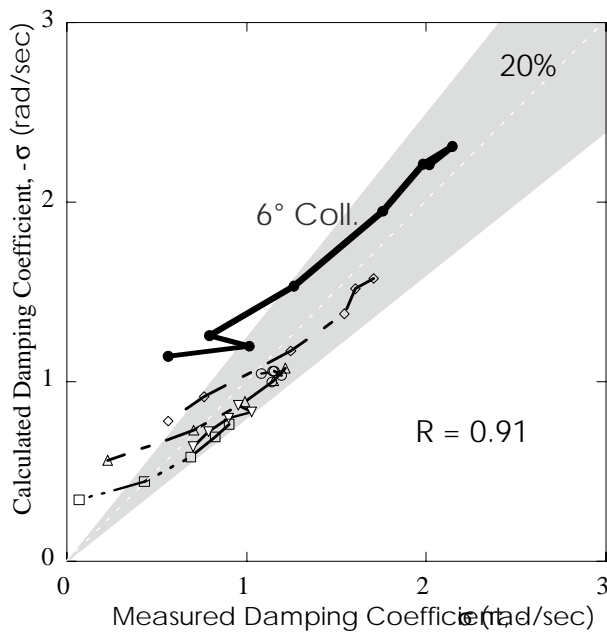
Fig. 3   Correlation of CAMRAD II analytical model with regressing lag mode damping measurements over a range of test conditions for the straight blade rotor in forward flight.
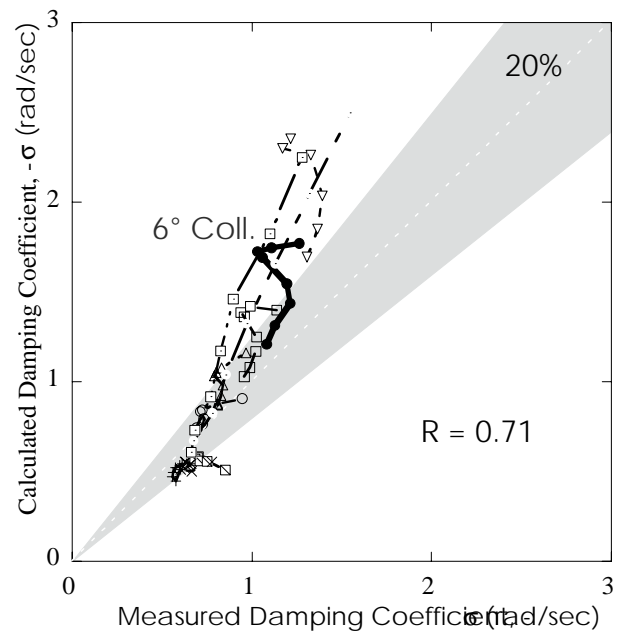
Fig. 4   Correlation of CAMRAD II analytical model with regressing lag mode damping measurements over a range of test conditions for the swept-tip rotor in forward flight.
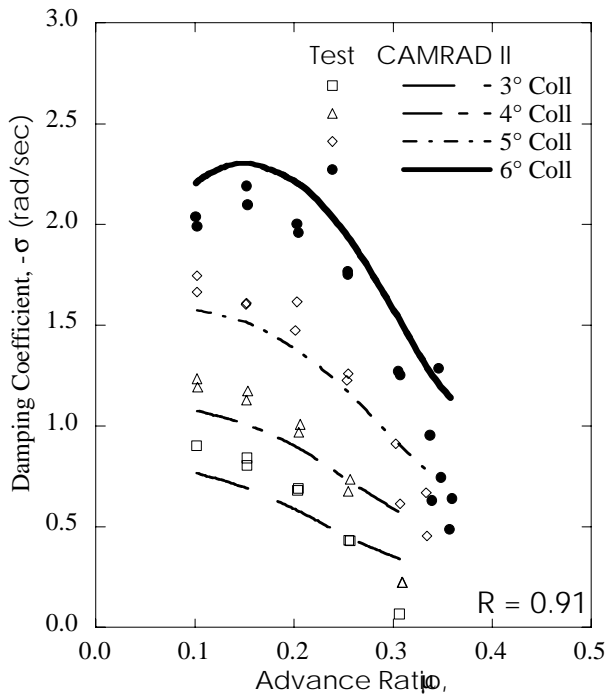
Fig. 5 Comparison of CAMRAD II analytical model with regressing lag mode damping measurements for straight blade rotor at four collective pitch angles with -6° shaft angle and 2° precone hub.
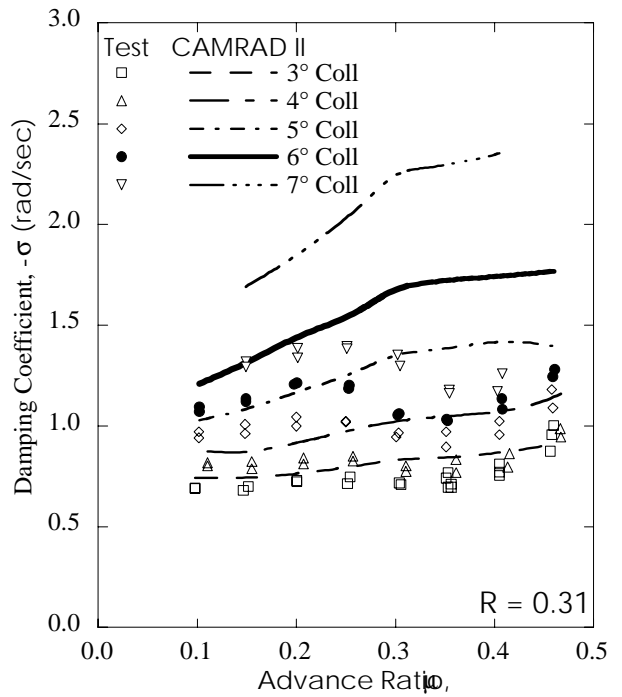
Fig. 6 Comparison of CAMRAD II analytical model with regressing lag mode damping measurements for swept-tip rotor at five collective pitch angles with 0° shaft angle and 0° precone hub.
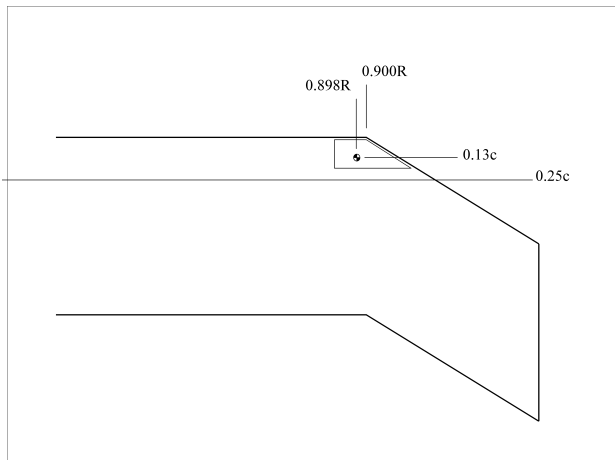
Fig. 7 Swept-tip rotor balance weight near blade tip.
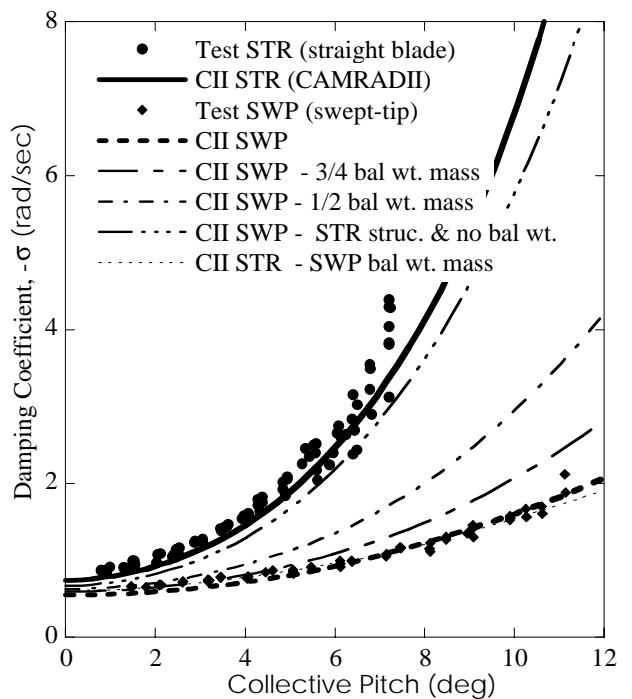
Fig. 8 Comparison of regressive lag mode damping measurements and CAMRAD II calculations for straight and swept-tip rotors in hover; 0° precone hub.
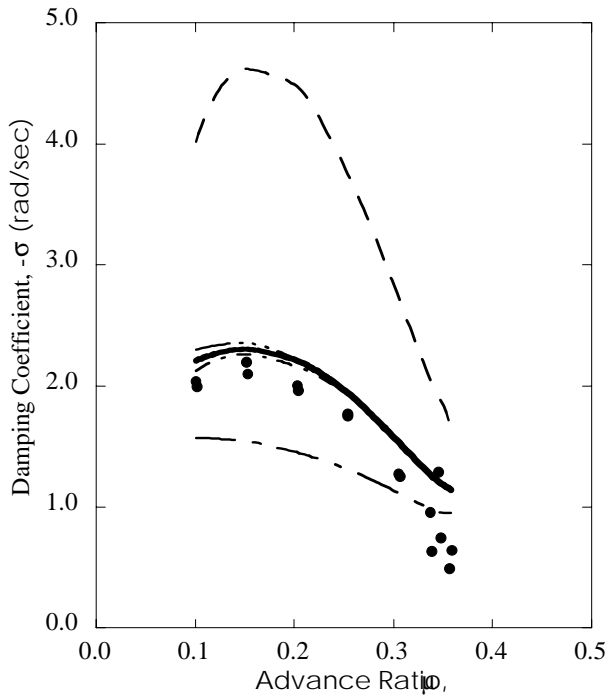
Fig. 9a Effect of center of gravity and tensile axis offsets on damping for straight blade rotor in forward flight; 6° collective pitch angle, -6° shaft angle, 2° precone.
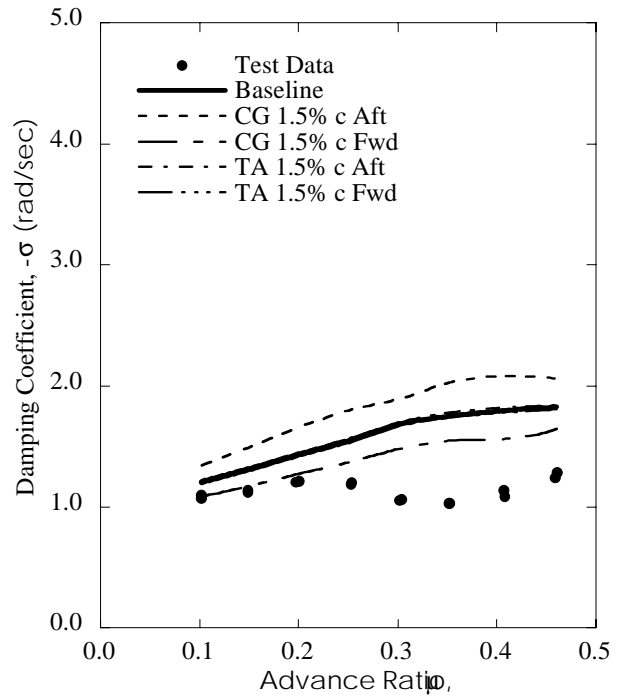
Fig. 9b Effect of center of gravity and tensile axis offsets on damping for swept-tip rotor in forward flight; 6° collective pitch angle, 0° shaft angle, 0° precone.
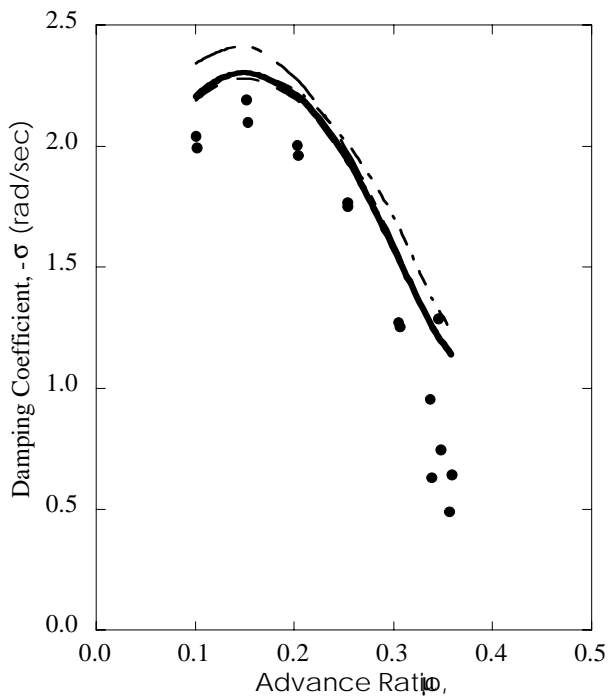
Fig. 10a Effect of flap, chord and torsion stiffness on damping for straight blade rotor in forward flight; 6° collective pitch angle, -6° shaft angle, 2° precone.
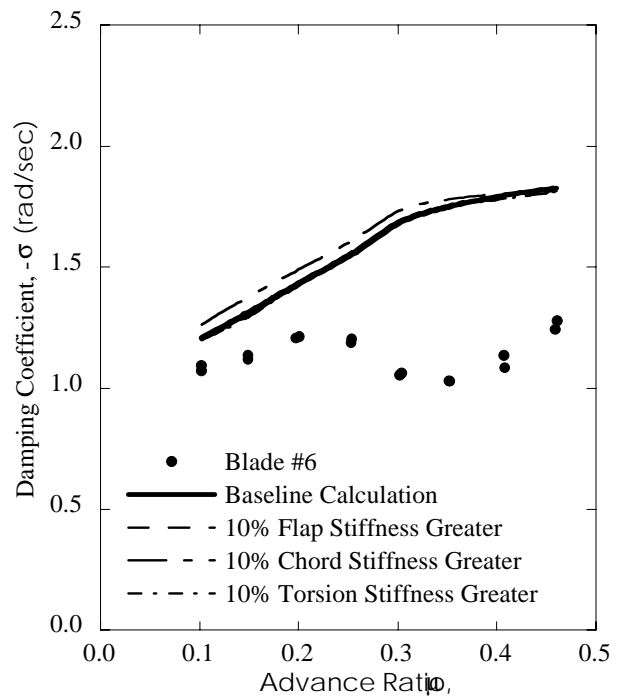
Fig. 10b Effect of flap, chord and torsion stiffness on damping for swept-tip rotor in forward flight; 6° collective pitch angle, 0° shaft angle, 0° precone.
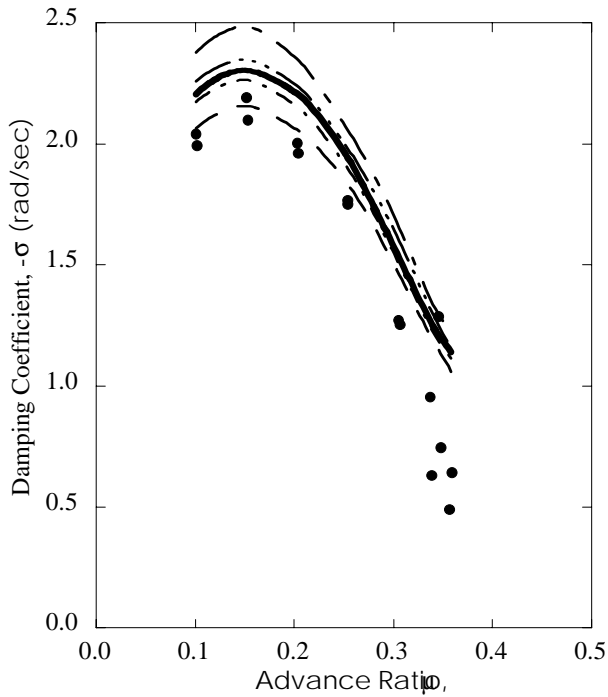
Fig. 11a Effect of mass and polar moment of inertia on damping for straight blade rotor in forward flight; 6° collective pitch angle, -6° shaft angle, 2° precone.
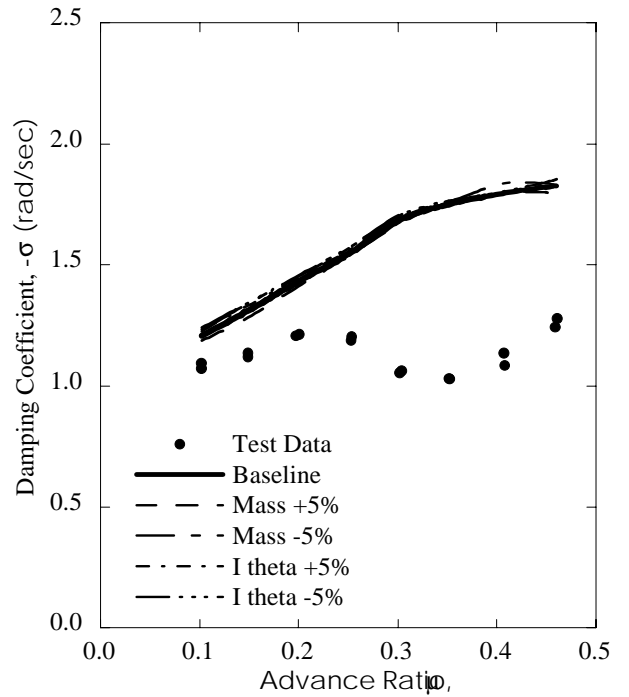
Fig. 11b Effect of mass and polar moment of inertia on damping for swept-tip rotor in forward flight; 6° collective pitch angle, 0° shaft angle, 0° precone.
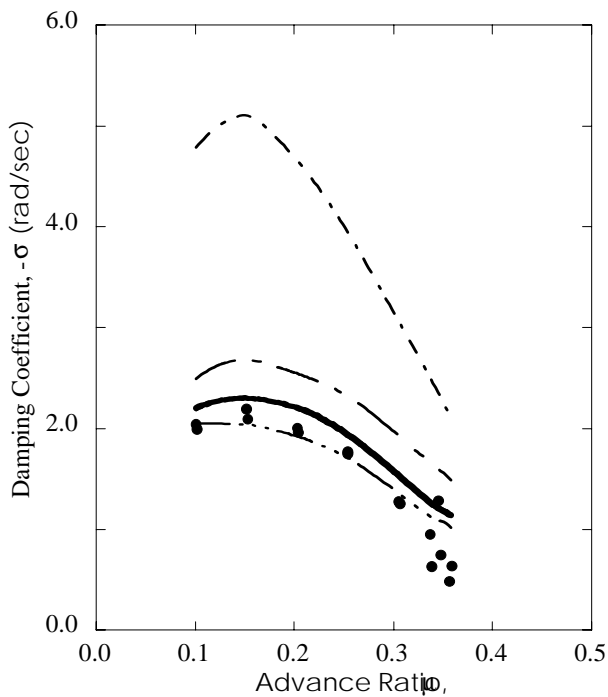
Fig. 12a Effect of sweep, droop, and torque offset on damping for straight blade rotor in forward flight; 6° collective pitch angle, -6° shaft angle, 2° precone.
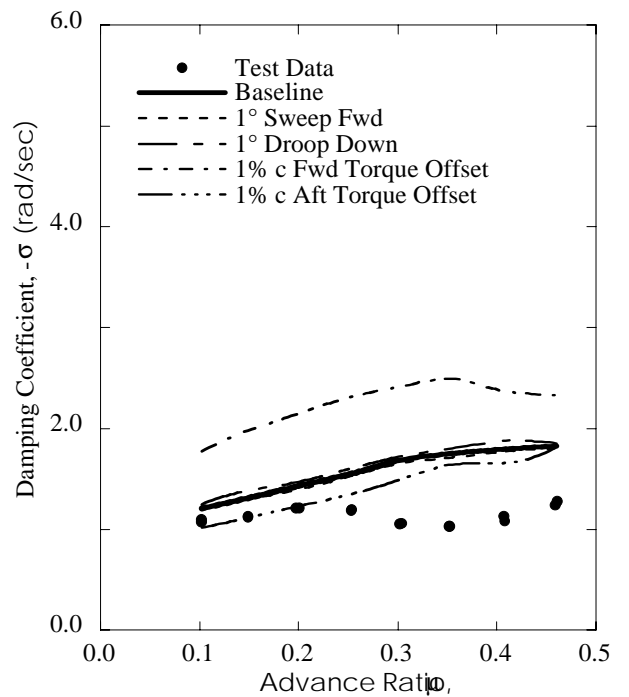
Fig. 12b Effect of sweep, droop, and torque offset on damping for swept-tip rotor in forward flight; 6° collective pitch angle, 0° shaft angle, 0° precone.
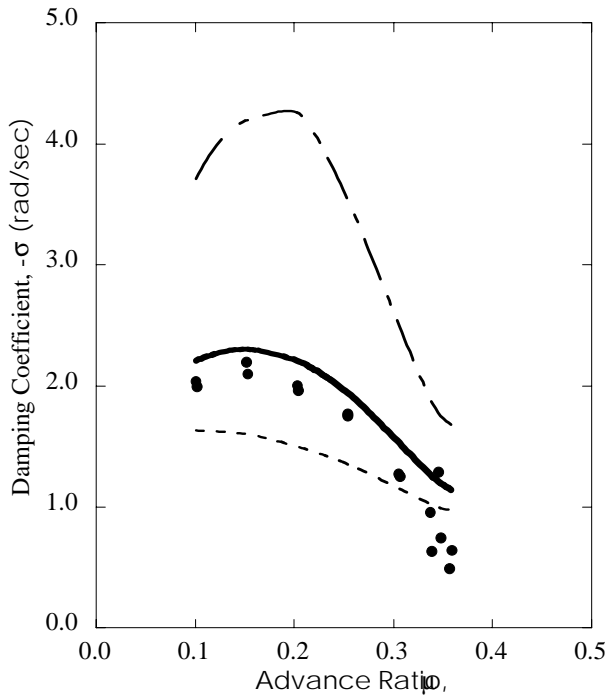
Fig. 13a **Effect of the aerodynamic center location on damping for straight blade rotor in forward flight; 6° collective pitch angle, -6° shaft angle, 2° precone.**
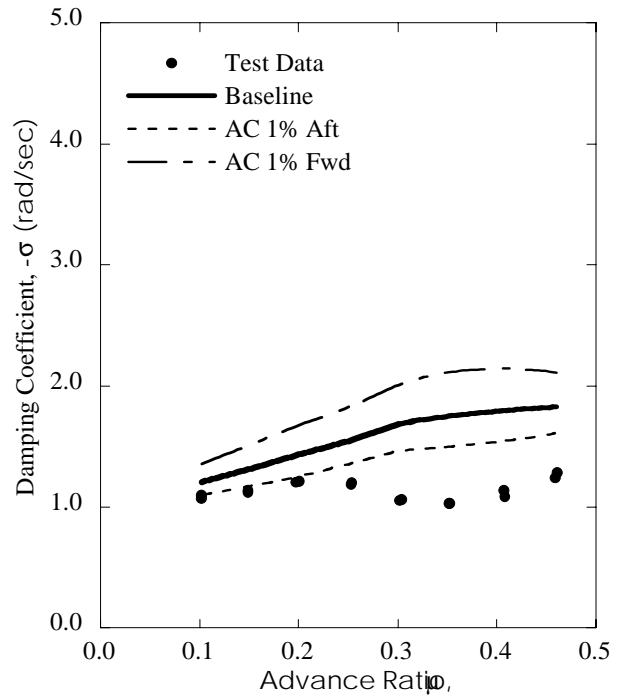
Fig. 13b **Effect of the aerodynamic center location on damping for swept-tip rotor in forward flight; 6° collective pitch angle, 0° shaft angle, 0° precone.**
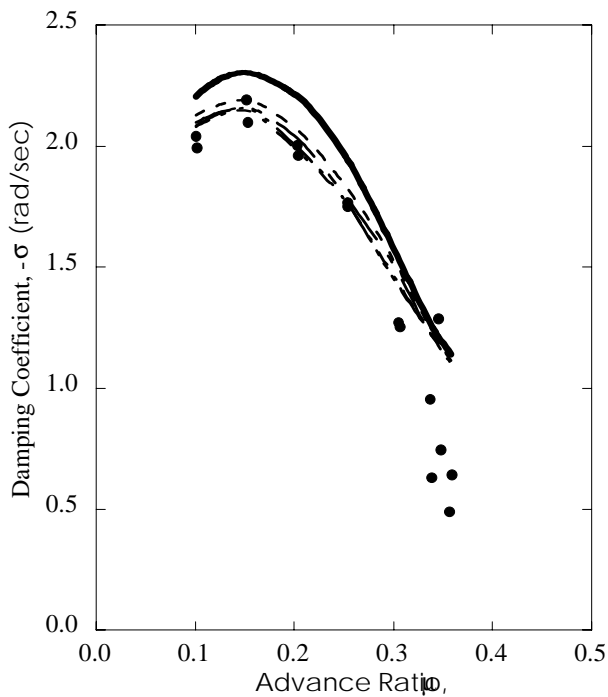
Fig. 14a **Effect of the number of structural elements on damping for straight blade rotor in forward flight; 6° collective pitch angle, -6° shaft angle, 2° precone.**
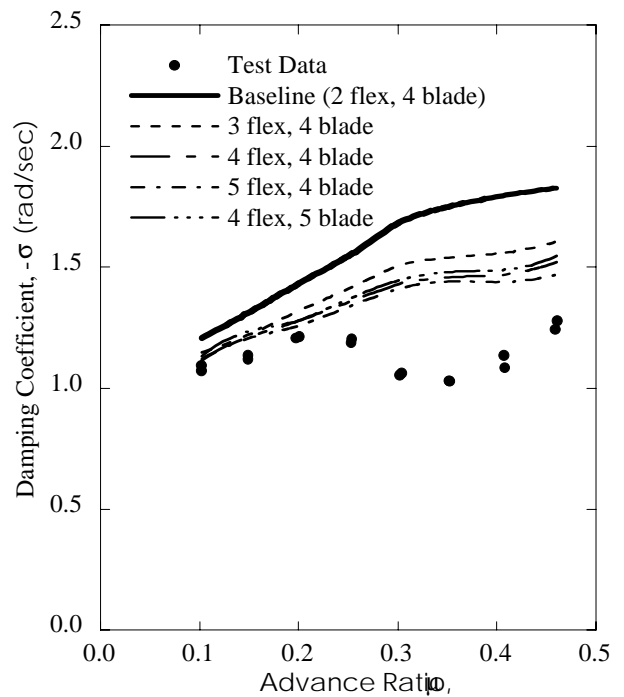
Fig. 14b **Effect of the number of structural elements on damping for swept-tip rotor in forward flight; 6° collective pitch angle, 0° shaft angle, 0° precone.**
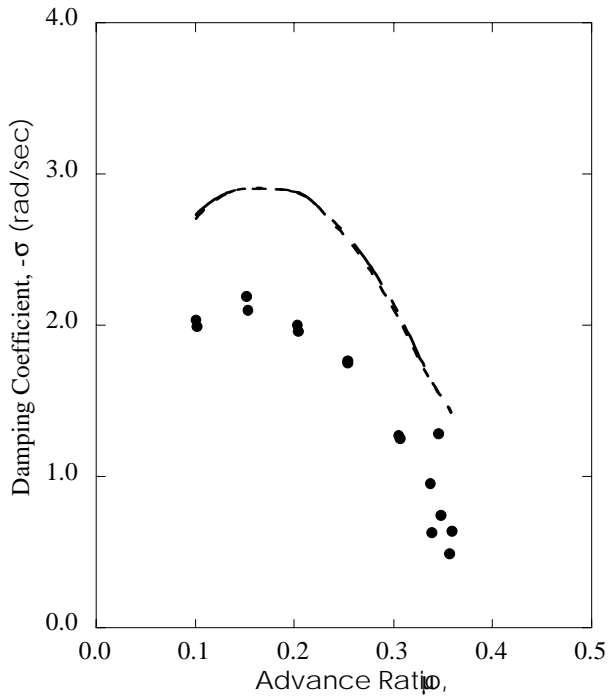
Fig. 15a Effect of dynamic inflow on damping for straight blade rotor in forward flight; 6° collective pitch angle, -6° shaft angle, 2° precone.
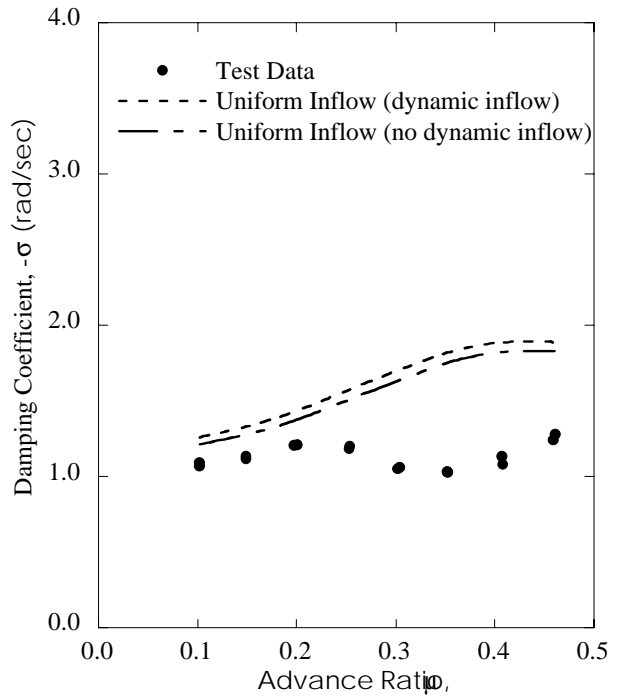
Fig. 15b Effect of dynamic inflow on damping for swept-tip rotor in forward flight; 6° collective pitch angle, 0° shaft angle, 0° precone.
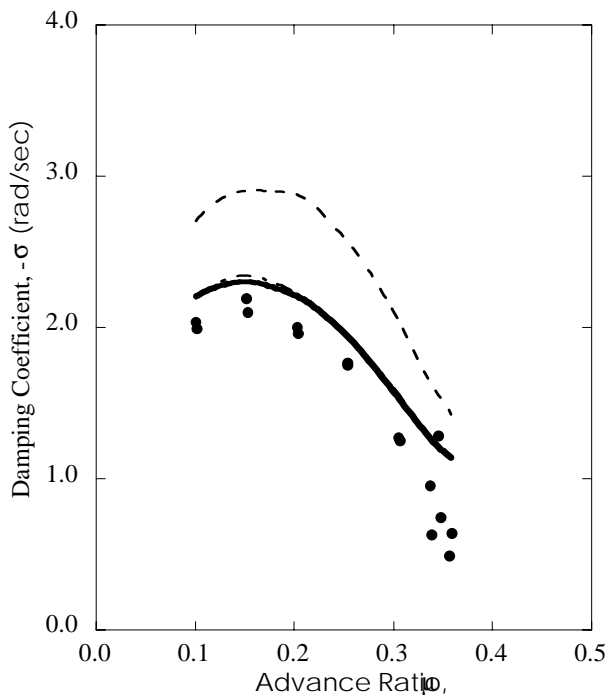
Fig. 16a Effect of the trim wake model on damping for straight blade rotor in forward flight; 6° collective pitch angle, -6° shaft angle, 2° precone.
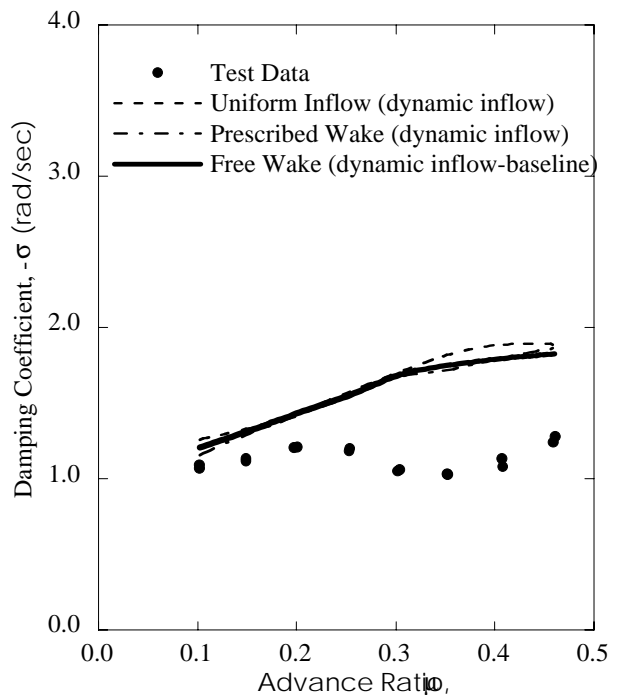
Fig. 16b Effect of the trim wake model on damping for swept-tip rotor in forward flight; 6° collective pitch angle, 0° shaft angle, 0° precone.
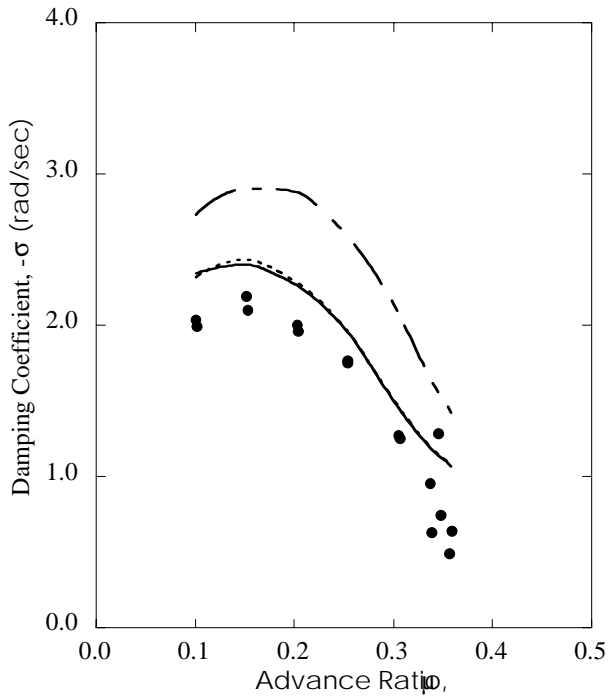
Fig. 17a Effect of the trim wake inflow velocity on damping for straight blade rotor in forward flight; 6° collective pitch angle, -6° shaft angle, 2° precone.
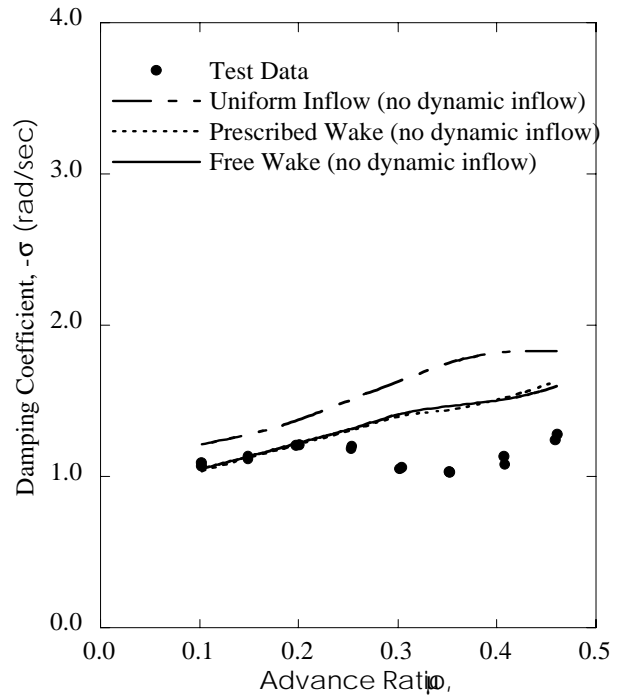
Fig. 17b Effect of the trim wake inflow velocity on damping for swept-tip rotor in forward flight; 6° collective pitch angle, 0° shaft angle, 0° precone.
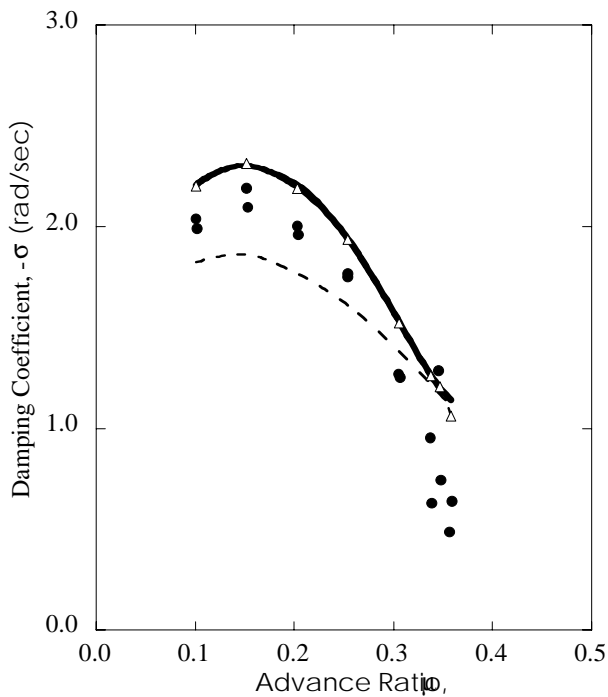
Fig. 18a Effect of incompressible aerodynamics and no stall models on damping for straight blade rotor in forward flight; 6° collective pitch angle, -6° shaft angle, 2° precone.
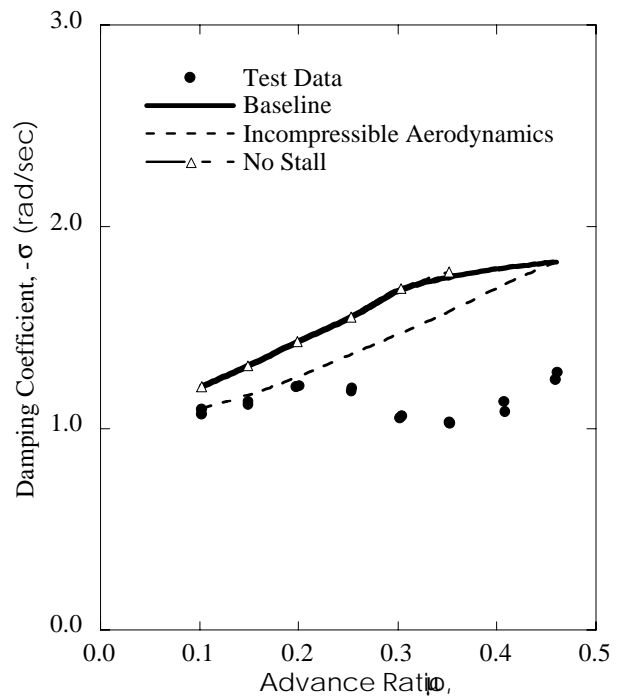
Fig. 18b Effect of incompressible aerodynamics and no stall models for swept-tip rotor in forward flight; 6° collective pitch angle, 0° shaft angle, 0° precone.
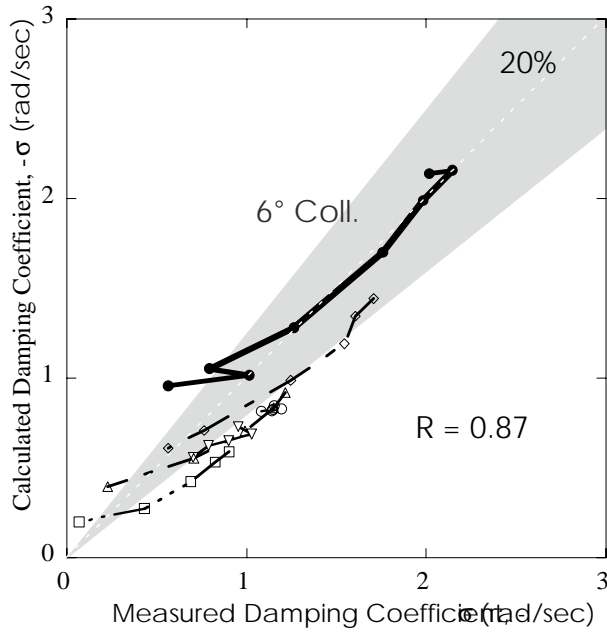
Fig. 19 Correlation of improved CAMRAD II analytical model with regressing lag mode damping measurements over a range of test conditions for the straight blade rotor in forward flight.
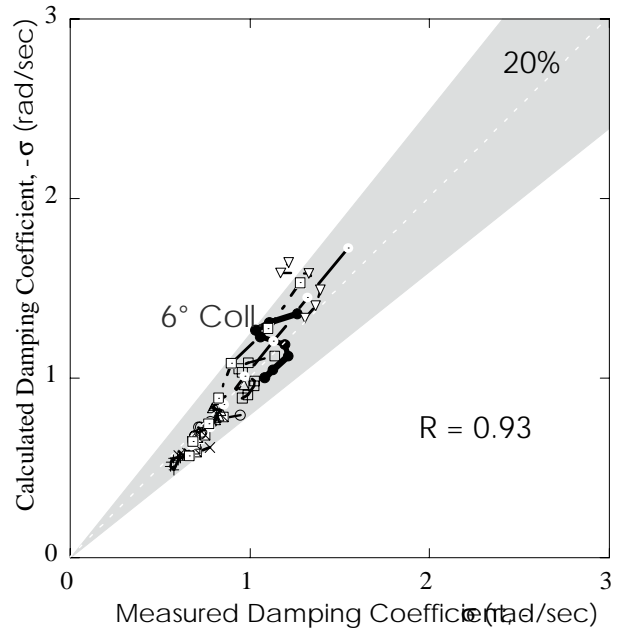
Fig. 20 Correlation of improved CAMRAD II analytical model with regressing lag mode damping measurements over a range of test conditions for the swept-tip rotor in forward flight.
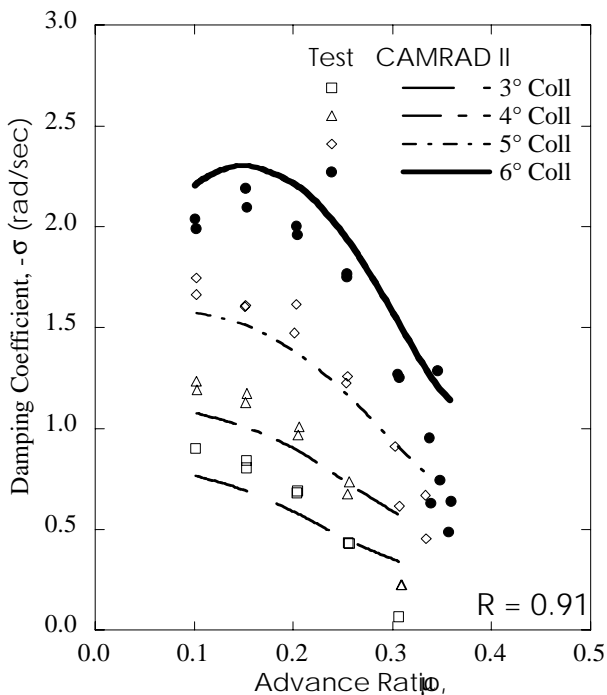
Fig. 21 Comparison of improved CAMRAD II analytical model with regressing lag mode damping measurements for straight blade rotor at four collective pitch angles with -6° shaft angle and 2° precone hub.

Fig. 22 Comparison of improved CAMRAD II analytical model with regressing lag mode damping measurements for swept-tip rotor at five collective pitch angles with 0° shaft angle and 0° precone hub.

7015